J Biomol NMR (2015) 61:55–64
DOI 10.1007/s10858-014-9882-7

ARTICLE

Utilization of paramagnetic relaxation enhancements for high-resolution NMR structure determination of a soluble loop-rich protein with sparse NOE distance restraints

Kyoko Furuita · Saori Kataoka · Toshihiko Sugiki · Yoshikazu Hattori · Naohiro Kobayashi · Takahisa Ikegami · Kazuhiro Shiozaki · Toshimichi Fujiwara · Chojiro Kojima

Received: 26 April 2014 / Accepted: 19 November 2014 / Published online: 27 November 2014

Abstract NMR structure determination of soluble proteins depends in large part on distance restraints derived from NOE. In this study, we examined the impact of paramagnetic relaxation enhancement (PRE)-derived distance restraints on protein structure determination. A high-resolution structure of the loop-rich soluble protein Sin1 could not be determined by conventional NOE-based procedures due to an insufficient number of NOE restraints. By using the 867 PRE-derived distance restraints obtained from the NOE-based structure determination procedure, a high-resolution structure of Sin1 could be successfully determined. The convergence and accuracy of the determined structure were improved by increasing the number of PRE-derived distance restraints. This study demonstrates that PRE-derived distance restraints are useful in the determination of a high-resolution structure of a soluble protein when the number of NOE constraints is insufficient.

Keywords Paramagnetic relaxation enhancement · PRE · Structure determination · Soluble protein · RDC · Sin1

The authors Kyoko Furuita and Saori Kataoka have been contributed equally to this work.

Electronic supplementary material The online version of this article (doi:10.1007/s10858-014-9882-7) contains supplementary material, which is available to authorized users.

K. Furuita · S. Kataoka · T. Sugiki · Y. Hattori · N. Kobayashi · T. Ikegami · T. Fujiwara · C. Kojima (✉)
Institute for Protein Research, Osaka University, 3-2 Yamadaoka, Suita, Osaka 565-0871, Japan
e-mail: kojima@protein.osaka-u.ac.jp

K. Shiozaki
Graduate School of Biological Sciences, Nara Institute of Science and Technology, 8916-5 Takayama, Ikoma, Nara 630-0192, Japan

Introduction

For high-resolution NMR structure determinations, especially for using an automated NOE signal assignment procedure that is becoming popular, a sufficient number of NOE peaks with nearly complete and accurate assignments are required. These requirements cannot always be met, and depend on the nature of the target protein being examined. Widely used computational programs, such as CYANA (Güntert et al. 1997; Herrmann et al. 2002), ARIA (Nilges et al. 1997) and autoStructure (Huang et al. 2003), can determine using the automated NOE signal assignment procedure. In the case of CYANA, more than 8.4 NOE restraints per residue and more than 90 % of chemical shift assignments are necessary for a successful NMR structure determination using the automated NOE assignment procedure (Jee and Güntert 2003). For membrane proteins and loop-rich proteins, these requirements are hardly met.

Paramagnetic relaxation enhancement (PRE)-derived distance restraints are easily obtained using spin labels. Spin labels contain a stable lone-pair electron, and are attached to target proteins at specific sites. The lone-pair electron enhances R_2 relaxation rates of NMR active nuclei, and the distances between the spin-labeled moiety and the NMR active nuclei are determined from enhancements of the R_2 relaxation rates. PRE provides semi-quantitative distance information in the range of 15–24 Å. Although PRE can provide longer distance information compared with NOE, it is less precise due to the flexibility of the attached spin-labeled moiety and de-localization of the lone-pair electron.

PRE is effective in accurately determining the global fold of a protein with a limited NOE data set (Battiste and Wagner 2000). A number of comprehensive studies that use PREs for structural analysis of proteins have been performed (Liang et al. 2006; Volkov et al. 2006; Clore et al. 2007; Clore and

Iwahara 2009; Simon et al. 2010; Madl et al. 2011). Recently, PRE has been utilized to determine inter-domain orientation and dimer interfaces (Madl et al. 2010; Yang et al. 2010), and the tertiary structure of membrane proteins in detergent micelles (Roosild et al. 2005; Zhou et al. 2008; Van Horn et al. 2009; Reckel et al. 2011). Detailed analyses of the influence of PRE-derived distance restraints on structure determinations have been reported for α-helical membrane proteins using simulated NMR data (Gottstein et al. 2012). It was reported that the number and location of spin labels affected the resulting protein structures. However, to our knowledge, the influence of PRE-derived distance restraints on high-resolution structure determinations of soluble proteins has not been investigated.

SAPK-interacting protein 1 (Sin1) is a subunit of the target of rapamycin (TOR) complex 2 (TORC2) (Frias et al. 2006; Jacinto et al. 2006; Yang et al. 2006). TOR is a serine/threonine-specific protein kinase, and the composition of TORC2 is conserved from yeast to humans (Cybulski and Hall 2009). Mammalian TORC2 (mTORC2) activates AGC-family protein kinases, such as Akt (protein kinase B), protein kinase Cα and SGK1, suggesting that mTORC2 may play a role in the regulation of cellular metabolism and proliferation (Hresko and Mueckler 2005; Sarbassov et al. 2005; Wullschleger et al. 2006; Facchinetti et al. 2008; García-Martínez and Alessi 2008; Cybulski and Hall 2009). In the fission yeast *Schizosaccharomyces pombe*, TORC2 activates the AGC-family kinase Gad8 (Matsuo et al. 2003; Ikeda et al. 2008). The conserved region in the middle domain of Sin1 ($Sin1_{CRIM}$) binds specifically to Gad8 (Tatebe et al. in preparation), and recruits Gad8 to TORC2 for phosphorylation and subsequent initiation of downstream signal transduction. Based on NMR chemical shift values of $Sin1_{CRIM}$ reported by our group (Kataoka et al. 2014), more than half of the residues of $Sin1_{CRIM}$ protein were estimated to be located within loops.

In this report, the impact of PRE-derived distance restraints on the NMR structure determination of the loop-rich soluble protein $Sin1_{CRIM}$ is described. Following application of the conventional NOE-based structure determination procedure to determine the structure of $Sin1_{CRIM}$, PRE-derived distance restrains were included in the NOE-based structure calculations. The impact of PRE-derived distance restraints on the structure determination was further investigated by changing the number of PRE- and NOE-derived distance restraints.

Materials and methods

Sample preparation of $Sin1_{CRIM}$ protein

A pCold-GST expression vector (Hayashi and Kojima 2008) encoding the *S. pombe* Sin1 CRIM domain (amino acids 247–400), designated as $Sin1_{CRIM}$ in this paper, was constructed as previously reported (Kataoka et al. 2014). This was utilized for the expression, purification and preparation of non-labeled, ^{15}N-labeled and ^{13}C, ^{15}N-labeled protein samples. Details of the protein sample preparation are provided in supplementary materials and methods.

Cysteine mutagenesis and spin-labeling of $Sin1_{CRIM}$ mutants

Single cysteine mutations of $Sin1_{CRIM}$ were introduced by the QuikChange site-directed mutagenesis method (Stratagene). Mutation sites were mostly selected from Ser/Thr residues, polar Arg/Lys/Asp/Glu/Gln residues expected to locate on the surface, and other Phe/Tyr/Leu/Val/Ala/Gly residues located on the edge of the secondary structure. Mutated ^{15}N-labeled $Sin1_{CRIM}$ proteins were overexpressed and purified by the same procedure utilized for the wild-type protein, except that the buffer used in the final size-exclusion column chromatography (SEC) did not contain DTT. Following purification, the spin-labeled reagent MTSL [(1-oxyl-2,2,5,5-tetramethyl-·3-pyrroline-3-methyl) methanethiosulfonate] was attached to the thiol moiety of the introduced cysteine residues by mixing MTSL with mutant $Sin1_{CRIM}$ samples (0.1 mM) at a 10:1 (MTSL:protein) molar ratio and then incubating the mixture at 20 °C for 4 h. Unreacted MTSL was carefully removed by SEC. The conjugation of MTSL was confirmed by mass spectroscopy before and after the collection of both paramagnetic and diamagnetic NMR data. When the incomplete spin labeling was found, its NMR data were not used for the analysis. $Sin1_{CRIM}$ and spin-labeled $Sin1_{CRIM}$ mutants were monomer evaluated by SEC.

NMR sample preparation

NMR samples of $Sin1_{CRIM}$ for resonance assignments and NOESY measurements were prepared at a protein concentration of 0.5 mM in 90/10 % H_2O/D_2O containing 50 mM potassium phosphate (pH 6.8), 50 mM KCl and 1 mM DTT. For PRE measurements, NMR samples were prepared at a protein concentration of 0.1 mM to avoid contributions from additional undesired PREs arising from random "elastic" collisions between a molecule and the paramagnetic group of another molecule (Clore and Iwahara 2009). In fact, for spin-labeled K312C mutant, the peak intensity of $^{1}H–^{15}N$ HSQC at 0.2 mM was 10 % lower than the expected, indicating the presence of non-specific intermolecular interactions at 0.2 mM (Figure S1). Following collection of paramagnetic NMR data, MTSL was reduced by addition of a threefold molar excess of ascorbic acid into the NMR sample in order to collect

diamagnetic NMR data. The reduction reaction was performed at 25 °C for more than an hour. NMR sample for residual dipolar coupling (RDC) measurements was prepared at a protein concentration of 70 μM in 90/10 % H_2O/D_2O containing 50 mM potassium phosphate (pH 6.8), 50 mM KCl, 1 mM DTT, and in the absence or presence of ~15 mg/ml Pf1 phage (ASLA Biotech Ltd). The NMR sample containing Pf1 phage was incubated at 4 °C for 12 h, and magnetically aligned in the NMR magnet at 30 °C for 5 h prior to the NMR measurement.

NMR measurements and analyses

NMR experiments were performed using an AVANCE I 800 MHz spectrometer or an AVANCE III 950 MHz spectrometer (Bruker). Spectra measured for resonance assignments were as previously described (Kataoka et al. 2014). To obtain distance restraints, ^{13}C-edited NOESY (Muhandiram et al. 1993) and ^{15}N-edited NOESY spectra (Zhang et al. 1994) were recorded. To obtain PRE distance restraints, ^{1}H–^{15}N HSQC spectra of MTSL-conjugated proteins in the paramagnetic and diamagnetic state were recorded. To obtain χ_1 angle restraints, three bond $J_{C'C}$ and $J_{NC'}$ coupling constants (Hu and Bax 1997) were measured. {^{1}H–^{15}N} heteronuclear NOE spectra were measured with and without 3 s of proton pre-saturation in an interleaved fashion (Farrow et al. 1994). ^{1}H–^{15}N RDCs were measured using in-phase and anti-phase ^{1}H–^{15}N HSQC pulse sequences under both isotropic and anisotropic conditions (Ottiger et al. 1998).

Uniformly sampled NMR spectra were processed using NMRPipe (Delaglio et al. 1995), while non-uniformly sampled (NUS) NMR spectra were processed using the Rowland NMR tool kit (http://rnmrtk.uchc.edu/rnmrtk/RNMRTK.html). Spectra were analyzed using Magro NMRView (http://bmrbdep.protein.osaka-u.ac.jp/en/nmrtoolbox/magro_nmrview.html) (Johnson and Blevins 1994; Kobayashi et al. 2007) and Sparky 3.115 (Goddard and Kneller 2008).

Chemical shift assignments of $Sin1_{CRIM}$ have been previously described in detail (Kataoka et al. 2014; BMRB accession code 11546). Resonances for 94 % of the backbone $^{1}H^{N}$ and ^{15}N, 92 % of ^{13}C', 95 % of $^{13}C\alpha$, 91 % of $^{1}H\alpha$, 72 % of side-chain ^{1}H and 69 % of side-chain ^{13}C were assigned. Backbone torsion angle restraints were estimated using the program TALOS+ (Shen et al. 2009). Chemical shift assignments of spin-labeled $Sin1_{CRIM}$ were from the wild-type $Sin1_{CRIM}$ comparing the HSQC spectra, simply the nearest cross peak.

PRE-derived distance restraints

PRE-derived distance restraints were calculated from intensity ratios of ^{1}H–^{15}N HSQC spectra in the paramagnetic and diamagnetic states (Figures S2 and S3) by the method introduced by (Battiste and Wagner 2000). The ^{1}H–^{15}N HSQC spectra were recorded within 90 min for each, since the spin labeled samples were not stable (Figure S4). Details of the PRE-derived distance calculations are provided in supplementary materials and methods.

PRE-derived distance restraints were classified into three types; (1) Peaks with an intensity ratio < 0.8 and detectable in the oxidized spectra, (2) severely broadened peaks and not detectable in the oxidized spectra, and (3) peaks with an intensity ratio >0.8. Peaks in class (1) were restrained as the calculated distance. Peaks in class (2) were restrained with no lower distance limit and upper distance limits of distances estimated from the noise level. Peaks in class (3) were restrained with no upper distance limit and lower distance limits of distances (11 Å for R291C and K321C and 10 Å for others) calculated from intensity ratio of 0.8 considering experimental errors. PRE-derived distance restraints were introduced between amide protons and C^{β} atoms of residues which were replaced by cysteine for the paramagnetic labeling (Reckel et al. 2011; Gottstein et al. 2012), with an error of ±7 Å. The flexibility was not considered here as a first approach. The concentration dependence of the PREs of the spin-labeled K312C mutant did not show the significant intermolecular PREs (Figure S5).

Structure calculation

Structure calculations and automated NOE assignments were performed using CYANA 3.95 (Güntert et al. 1997; Herrmann et al. 2002). Fifty structures were calculated, and ten structures with the lowest target function were selected for evaluation of the structural quality and treated as representative. When structure calculations were combined with automated NOE assignments, the NOE peaks were automatically assigned in seven cycles of the structure calculations, and NOE assignment tables were utilized for the final structure calculation. Fifty structures were calculated and ten structures with the lowest target function were selected in each cycle. Details of the structure calculations are provided in supplementary materials and methods. The atomic coordinates of the refined structures of $Sin1_{CRIM}$ have been deposited in the Protein Data Bank with accession code 2RUJ.

Validation of calculated structure

Determined structures were validated by examining Pearson's linear correlation coefficient between experimental RDC values and back-calculated RDC values obtained from the structures using the program PALES (Zweckstetter and Bax 2000). Experimental RDC values were measured using the nmrDraw program (Delaglio et al.

1995). Only RDC values of residues that were classified as being located in helix or extended regions by the TALOS+ program were employed for the validation procedure.

Results

Secondary structure and dynamics of $Sin1_{CRIM}$

The relationship between the secondary structure and the dynamics was investigated for $Sin1_{CRIM}$. The $^{1}H–^{15}N$ heteronuclear NOE values of both N- and C-terminal regions of $Sin1_{CRIM}$ (amino acids 247–273 and 396–400) were below 0.6, indicating that both N- and C-terminal regions are flexible (Fig. 1) (Kay et al. 1989). For the central region (amino acids 274–395), the $^{1}H–^{15}N$ heteronuclear NOE values were above 0.6, indicating that the central region is structurally ordered. The secondary structure was estimated by the backbone dihedral angles evaluated by the TALOS+ program (Shen et al. 2009). The central region had a low content of secondary structure elements, and more than half of the residues were located in loop regions (Fig. 1). That is, $Sin1_{CRIM}$ is a highly loop-rich protein, although these loops are inflexible and structurally ordered.

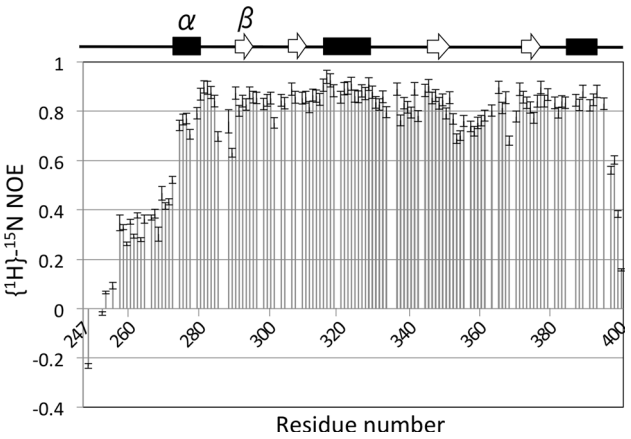

Fig. 1 $\{^{1}H–^{15}N\}$ heteronuclear NOE values of $Sin1_{CRIM}$. Residue numbers are denoted on the *horizontal axis*. The secondary structure elements of $Sin1_{CRIM}$ determined by the program TALOS+ are shown above the graph. Errors for NOE values were estimated by a Monte Carlo procedure

Structure calculation without PRE-derived distance restraints

The structure of $Sin1_{CRIM}$ was calculated using a conventional NOE-based procedure, and combined with automated NOE assignments using the program CYANA. However, the calculated structures were not converged sufficiently, mainly due to the insufficient number (>1,000) of NOE restraints (Fig. 2; Table 1). The backbone root mean square deviation (RMSD) values of the ordered region (amino acids 275–395) and the correlation coefficient between experimental and back-calculated RDC values using the calculated structures were 3.06 ± 0.89 and 0.56 ± 0.12 Å, respectively (Table 1).

Although most $^{1}H–^{15}N$ HSQC peaks of $Sin1_{CRIM}$ were well resolved with high signal intensities (Fig. 3), many signals in the 3D NMR spectra were weakened or disappeared. For example, in the H(CCO)NH and C(CO)NH spectra, many signals were not observed, which imposed a limit on the signal assignments of side-chain chemical shifts (~70 %), and the ^{13}C- and ^{15}N-edited NOESY spectra could not be measured with high signal-to-noise (S/N) ratio. Additionally, the NMR sample of $Sin1_{CRIM}$ precipitated within 3 days of the NMR measurements at 30 °C. These experimental limitations made the structure determination difficult.

Site-directed spin labeling and PRE-derived distance restraints

Since the high-resolution structure of $Sin1_{CRIM}$ could not be determined by a conventional NOE-based procedure, PRE-derived distance restrains were employed. In order to

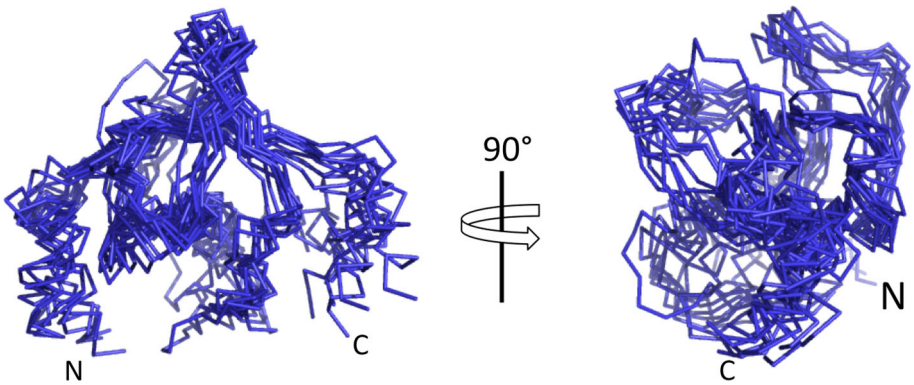

Fig. 2 Superimposition of the final ten structures calculated by the program CYANA combined with automated NOE assignments in the absence of PRE distance restraints

Table 1 Structural statistics of $Sin1_{CRIM}$

	In the absence of PRE	In the presence of PRE (nine spin-labeled)
NOESY peaks		
^{13}C	3,911	
^{15}N	1,250	
Total	5,161	
Completeness of chemical shift assignments	84.8 %	
Dihedral angle restraints		
φ	110	
ϕ	90	
χ1	12	
PRE distance restraints		
Upper	0	163
Lower	0	704
Total	0	867
NOE distance restraints		
Short $\|i - j\| \leq 1$	645	636
Middle $1 < \|i - j\| \leq 5$	136	132
Long $5 \leq \|i - j\|$	143	199
Total	924	967
RMSD (amino acids 275–395) (Å)		
Backbone	3.06 ± 0.89	0.91 ± 0.17
All heavy	3.57 ± 0.84	1.37 ± 0.19
RDC correlation coefficient		
	0.56 ± 0.12	0.86 ± 0.05

obtain the PRE-derived distance restraints, 29 single cysteine mutants were designed for site-directed spin labeling using MTSL (Table S1). Fourteen of these mutants were successfully introduced into the $Sin1_{CRIM}$ gene by genetic engineering, and the respective recombinant proteins overexpressed and purified. Following conjugation of MTSL onto the thiol moiety of the cysteine residue, ^{1}H–^{15}N HSQC spectra were measured for each mutant under both paramagnetic and diamagnetic conditions. Following the NMR measurements, the conjunction of MTSL was confirmed by mass spectroscopy for all samples. Of the mutants generated, mutants S269C, Q331C, Q341C, R366C and S399C were not used to collect PRE-derived distance restraints (Fig. 3a). For S269C and S399C, the substituted cysteines were located in flexible regions (Fig. 1). For Q341C, marked chemical shift changes were observed for many peaks compared with wild-type (Figure S2). For Q331C, a ^{1}H–^{15}N HSQC spectrum with sufficient signal-to-noise ratio was not obtained (Figure S2). For R366C, the ^{1}H–^{15}N HSQC spectra of the paramagnetic and diamagnetic states differed significantly (Figure S2). For the residual 9 mutants (T280C, S282C, R291C, S301C, K312C, L332C, S371C, T384C and A394C), the distances between the lone spin of MTSL and amide protons were evaluated based on a comparison of the signal intensity ratios of the ^{1}H–^{15}N HSQC spectra of the paramagnetic and diamagnetic states (Figures 3 and S3). It is noted that PRE-derived distances for flexible residues, where the ^{1}H–^{15}N heteronuclear NOE values were below 0.6 (Kay et al. 1989) (Fig. 1), were not used for the structure calculations.

Structure calculation with PRE-derived distance restraints

About 100 PRE-derived distance restraints obtained from each mutant were used 'independently' for the structure calculation combined with the automated NOE assignments. A total of nine sets comprising about 100 PRE-derived distance restraints were obtained from nine mutants (Fig. 3a), however, no sufficient improvement in the RMSD values or RDC correlation coefficients of the calculated structures was achieved when each set of about 100 PRE-derived distance restraints was used 'independently' (Table S2). The location of the mutations and sets of PRE-derived distance restraints were widely dispersed over the $Sin1_{CRIM}$ molecule (Figs. 3a , S6). This result clearly suggests that about 100 PRE-derived distance restraints obtained from one single-site spin label were insufficient to improve the quality of the calculated protein structure.

All data obtained from the nine mutants were then used 'simultaneously' for the structure calculations combined with automated NOE assignments since each data set of about 100 PRE-derived distance restraints failed to improve the quality of the calculated structure. The total number of PRE-derived distance restraints employed was 867, comprising 163 upper and 704 lower distance limits. The accuracy and convergence of the calculated structures improved dramatically (Fig. 4; Table 1). The backbone RMSD values and the correlation coefficient between experimental and back-calculated RDC values using the calculated structures were 0.91 ± 0.17 and 0.86 ± 0.05 Å, respectively (Table 1 ; Figure S7).

The structure was further refined by Xplor-NIH (Schwieters et al. 2003, 2006). A superimposed picture of the refined structures and a ribbon representation of the lowest energy structure are shown in Figure S8, and the structural statistics is presented in Table S3. The structure of $Sin1_{CRIM}$ and its homologs have not been reported. The lowest energy structure was submitted to Dali server (Holm and Rosenström 2010) to find the similar structure. The most similar structures were Ubiquitin-fold modifier 1 (PDBID 1L7Y, Z-score = 5.4) and Ras binding domains from RalGDS (PDBID 1RAX, Z-score = 5.3 and PDBID 1LXD, Z-score = 5.1). These structures have ubiquitin-like

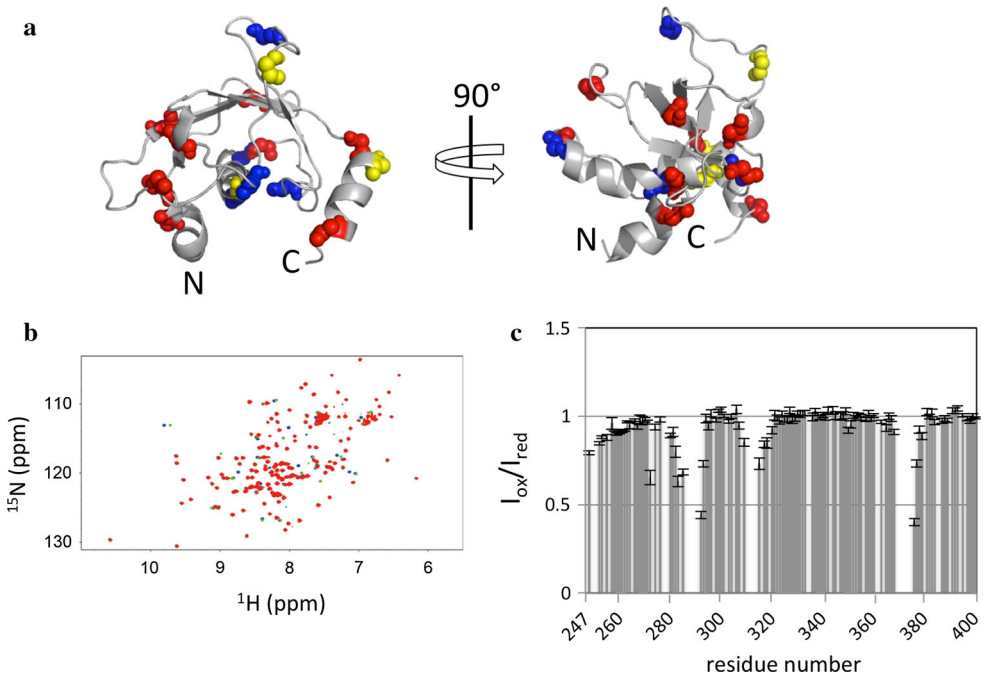

Fig. 3 Site-specific spin labeling of $Sin1_{CRIM}$ protein. **a** Spin-labeled sites on $Sin1_{CRIM}$ (amino acid 272–397). *Red spheres* indicate sites of spin labels from which PRE distance restraints were obtained and used for structure determination (T280, S282, R291, S301, K312, L332, S371, T384 and A394). *Yellow spheres* indicate sites of spin labels from which PRE distance restraints were obtained and not used for structure determination (S317, F361 and A386). *Blue spheres* indicate sites of spin labels from which PRE distance restraints could not be obtained (G321, Q331, Q341, G355 and R366). **b** An overlay of $^{1}H–^{15}N$ HSQC spectra of $Sin1_{CRIM}$ (WT) (*blue*), MTSL-conjugated $Sin1_{CRIM}$ (K312C) in the diamagnetic (*green*) and paramagnetic (*red*) states. **c** Intensity ratio of peaks calculated from $^{1}H–^{15}N$ HSQC spectra of $Sin1_{CRIM}$ (K312C) in the paramagnetic and diamagnetic states. *Error bars* indicate experimental uncertainties based on the noise level in the NMR spectra

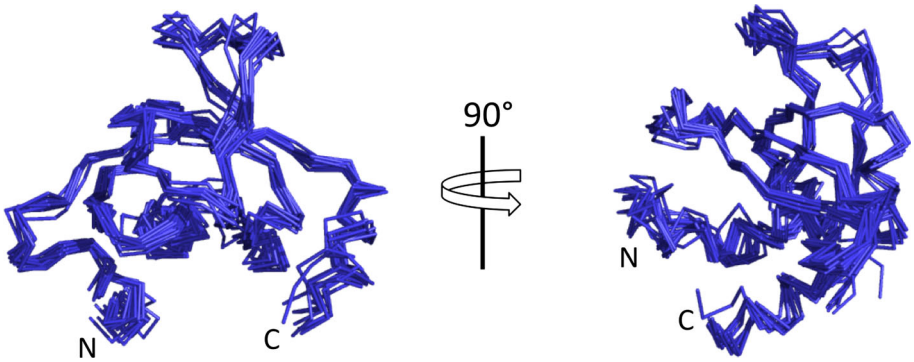

Fig. 4 Superimposition of the final ten structures calculated by the program CYANA combined with automated NOE assignments in the presence of PRE distance restraints

fold and belong to the ubiquitin-like superfamily on the SCOP database (Murzin et al. 1995). Since the structures possessing the Z-score above 2 have similar fold (Holm et al. 2008), $Sin1_{CRIM}$ seems to have ubiquitin-like fold.

Impact of PRE-derived distance restraints on structure determination

As described above, use of the PRE-derived distance restraints dramatically improved the determined NMR structure. In an effort to gain insight into the impact of PRE-derived distance restraints on the structure determination, the number of NOE-derived and PRE-derived distance restraints was depicted against residue number (Figs. 5 , S9). As shown by the black bars in Fig. 5a, the NOE-derived long-range distance restraints were found in the limited regions, around residues 320 and 380. Additionally, as shown by the gray bars in Fig. 5a, the number of NOE-derived distance restraints was relatively small in both the N-terminal (residues 247–300) and C-terminal (residues

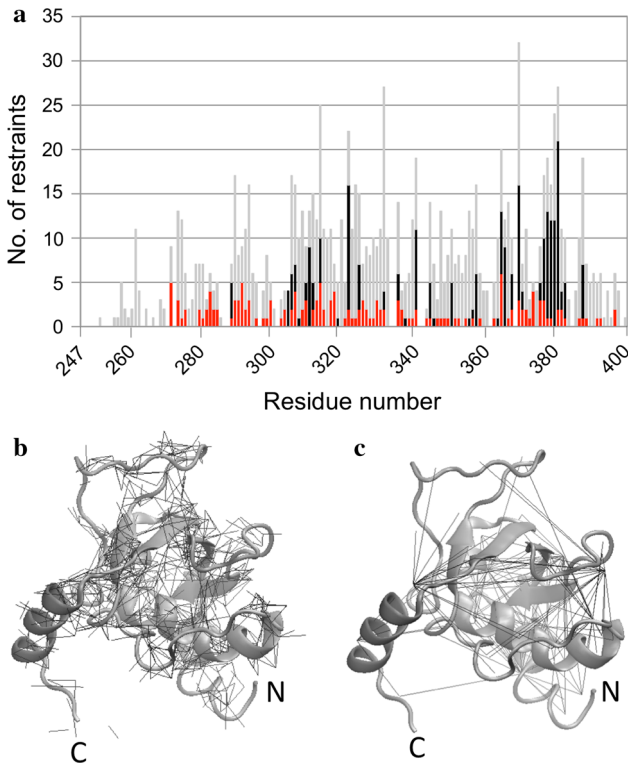

Fig. 5 NOE- and PRE-derived distance restraints. **a** The number of distance restraints for each residue that was used for the structure determination of $Sin1_{CRIM}$. PRE, Long-range NOE and other NOE are shown in *red, black* and *gray*, respectively. **b** The NOEs used for the structure determination are shown by lines on the lowest target function structure of $Sin1_{CRIM}$. **c** PREs used for the structure determination are shown by lines on the lowest target function structure of $Sin1_{CRIM}$

385–400) regions. On the other hand, as shown by the red bars in Fig. 5a, the PRE-derived upper distance limits were evenly found over the structured region, and complemented the lack of NOE-derived long-range distance restraints, especially in the N-terminal region (Fig. 5).

For the evaluation of the contribution of PRE-derived distance restraints on the structure determination, the structure calculations were repeated in the absence or presence of PRE-derived distance restraints using the same NOE-based upper distance limits. The distance restraints obtained from the final cycle and used to determine the structure are shown in Fig. 4. By employing the PRE-derived distance restraints, the RMSD values improved from 1.51 ± 0.59 to 0.98 ± 0.20 Å, and the correlation coefficient between the experimental RDC values and back-calculated RDC values obtained from the calculated structures improved from 0.59 ± 0.04 to 0.87 ± 0.05 (Fig. 6). This result indicates that PRE-derived distance restraints are reliable and can complement the insufficient NOE-based distance restraints, although the distance restraint is weak due to the large error range of ±7 Å.

Minimum number of PRE-derived distance restraints

For the evaluation of the minimum number of PRE-derived distance restraints, the number of PRE-derived distance restraints (163 and 704 of upper and lower distance limits, respectively) was randomly decreased in a stepwise manner (87.5, 75.0, 62.5, 50.0, 37.5, 25.0 and 12.5 %) and structure calculations were performed in each case. The convergence of the calculated structures and the correlation between the experimental and back-calculated RDC values decreased exponentially with decreasing number of PRE-derived distance restraints (Fig. 7). When decreasing the number of PRE-derived distance restraints by more than 50 %, the structure suddenly became dramatically worse.

In an effort to improve the structure further, an additional five single cysteine mutants (S317C, G321C, G355C, F361C and A386C) were designed based on the determined structure to increase the number of PRE-derived distance restraints. Of these mutants, G321C and G355C were not used to collect PRE-derived distance restraints since marked chemical shift changes were observed (Figure S2). Thus the PRE-derived distance restraints collected from the residual three mutants (S317C, F361C or A386C) were used in structure calculations to improve the structure (Figs. 3a , S6). However, the structure did not improve significantly by employing these additional constraints (Figure S10).

Discussion

PRE-derived distance restraints are useful for structure refinement of the soluble ordered loop-rich protein

PRE-derived distance restraints have been evaluated and utilized for the structure determination of soluble and membrane proteins (Battiste et al. 2000; Gottstein et al. 2012). In the case of soluble proteins, Battiste et al. (2000) have shown that PRE-derived distance restraints, in combination with HN–HN NOEs without hydrogen bond restraints, can determine the global fold of a soluble protein, where the protein structure was determined with a backbone RMSD of 2.3 Å. In the case of membrane proteins, Gottstein et al. (2012) have shown that PRE-derived distance restraints, in combination with limited NOEs and hydrogen bond restraints, could provide sufficient structural information for the accurate structure determination of an α-helical membrane protein. Here, we have shown that PRE-derived distance restraints, in combination with an insufficient number of NOEs without hydrogen bond restraints, can dramatically improve the structure of a soluble protein in terms of both accuracy and convergence, and resulting in a backbone RMSD of 0.91 Å (Fig. 4).

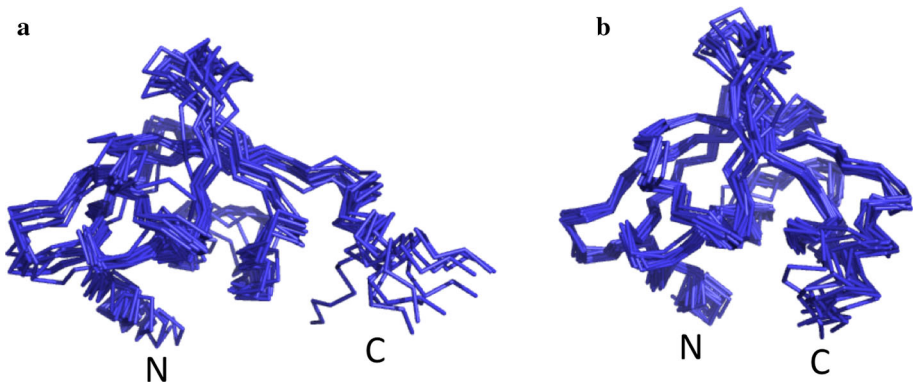

Fig. 6 Superimposition of the final ten structures calculated in the absence (**a**) or presence (**b**) of PRE-derived distance restraints. NOE upper distance limits, created through automated NOE assignments in the presence of PRE-derived distance restraints, were applied to both calculations

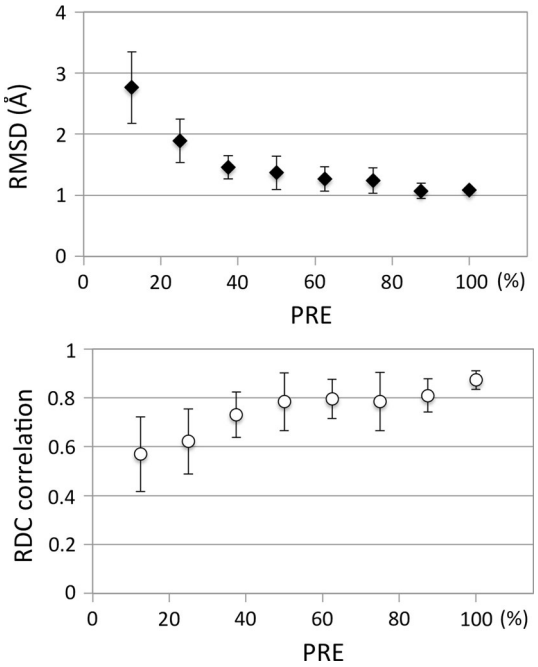

Fig. 7 Evaluation of effective minimum number of PRE. Structure calculations were performed using 12.5, 25.0, 37.5, 50.0, 62.5, 75.0, 87.5 and 100 % of the PRE-derived distance restraints. The RMSD values of backbone atoms and correlation coefficients between experimental and back-calculated RDC values using the calculate structures

Therefore, at least in the case of soluble proteins, the employment of PRE-distance restraints is useful in the determination of an accurate high-resolution structure.

In general, secondary structure elements and related hydrogen bond restraints are key factors in NMR structure determination of proteins. For example, for most membrane proteins, the secondary structure is fixed by dihedral angles and hydrogen bond restraints (Gottstein et al. 2012). Our target, $Sin1_{CRIM}$, is a structurally ordered loop-rich protein, and the content of the secondary structure elements is much lower than that found in other proteins. The hydrogen bond restraint is not used in the structure calculation since the hydrogen bond pair is not identified. In this sense, $Sin1_{CRIM}$ is not a good target for NMR structure determination using conventional procedures. Here, employment of a sufficient number of PRE-derived distance restraints dramatically improved the structure of $Sin1_{CRIM}$ in terms of both accuracy and convergence. Therefore, the use of PRE-derived distance restraints can facilitate the structure determination of structurally ordered loop-rich proteins.

Impact of PRE-derived distance restraints on automated NOE assignments

In the absence of PRE-derived distance restraints, with automated NOE assignments, the backbone RMSD value was 3.06 ± 0.89 Å and the correlation coefficient between experimental and back-calculated RDC values was 0.56 ± 0.12 (Fig. 2; Table 1). On the other hand, in the absence of PRE-derived distance restraints, with fixed NOE upper distance limits that were created by the CYANA automated assignment procedure in the presence of PRE-derived distance restrains, the RMSD value was 1.51 ± 0.59 Å and the correlation coefficient was 0.59 ± 0.04 (Fig. 6a). Although both calculations were performed in the absence of PRE-derived distance restraints, the RMSD values varied greatly. This difference is derived from the improvement in the automated NOE assignments by the PRE-derived distance restraints. The number of final NOE distance restraints increased from 924 to 967 by employing PRE-derived distance restraints, and the increased distance restraints were mostly long-range (Table 1 ; Figure S11). Additionally, the NOE distance restraints created without the PRE-derived distance restraints contained inappropriate restraints that were absent in those restraints created using the PRE-derived distance restraints. Therefore, in the automated NOE assignment process, the use of PRE-derived distance restraints led to an increase in the number of NOE-derived upper distance limits, especially long-range distance

restraints, and a decrease in the number of inappropriate restraints.

Conclusions

The present work shows that employment of PRE-derived distance restraints can contribute to the high-resolution NMR structure determination of proteins. Combined with conventional NOE-based procedures, the use of PRE-derived distance restraints significantly improved the convergence and accuracy of the determined structure. PRE-derived distance restraints could also be used in the automated NOE assignment process of CYANA. The PRE-assisted structure calculation procedure presented here can be utilized as a powerful option to determine the high-resolution NMR structure of proteins, especially in cases where chemical shift assignments and/or NOE data are insufficient.

Acknowledgments We thank Dr. Peter Güntert for letting us use CYANA 3.95. We thank Momoko Yoneyama, and Yuki Nishigaya for sample preparation and mass spectrometry measurements, respectively. This work was supported in part by Grants from MEXT/JSPS KAKENHI, TPRP, Platform for Drug Discovery, Informatics, and Structural Life Science to K.S., T.F. and C.K., and Grants-in-Aid for JSPS Fellows to K.F. and S.K.

References

Battiste JL, Wagner G (2000) Utilization of site-directed spin labeling and high-resolution heteronuclear nuclear magnetic resonance for global fold determination of large proteins with limited nuclear overhauser effect data. Biochemistry 39:5355–5365

Clore G, Iwahara J (2009) Theory, practice and applications of paramagnetic relaxation enhancement for the characterization of transient low-population states of biological macromolecules and their complexes. Chem Rev 109:4108–4139

Clore G, Tang C, Iwahara J (2007) Elucidating transient macromolecular interactions using paramagnetic relaxation enhancement. Curr Opin Struct Biol 17:603–616

Cybulski N, Hall MN (2009) TOR complex 2: a signaling pathway of its own. Trends Biochem Sci 34:620–627

Delaglio F, Grzesiek S, Vuister G, Zhu G, Pfeifer J, Bax A (1995) NMRPipe: a multidimensional spectral processing system based on UNIX pipes. J Biomol NMR 6:277–293

Facchinetti V, Ouyang W, Wei H, Soto N, Lazorchak A, Gould C, Lowry C, Newton AC, Mao Y, Miao RQ, Sessa WC, Qin J, Zhang P, Su B, Jacinto E (2008) The mammalian target of rapamycin complex 2 controls folding and stability of Akt and protein kinase C. EMBO J 27:1932–19243

Farrow N, Muhandiram R, Singer A, Pascal S, Kay C, Gish G, Shoelson S, Pawson T, Formankay J, Kay L (1994) Backbone dynamics of a free and a phosphopeptide-complexed Src Homology-2 domain studied by N-15 nmr relaxation. Biochemistry 33:5984–6003

Frias MA, Thoreen CC, Jaffe JD, Schroder W, Sculley T, Carr SA, Sabatini DM (2006) mSin1 is necessary for Akt/PKB phosphorylation, and its isoforms define three distinct mTORC2s. Curr Biol 16:1865–1870

García-Martínez JM, Alessi DR (2008) mTOR complex 2 (mTORC2) controls hydrophobic motif phosphorylation and activation of serum- and glucocorticoid-induced protein kinase 1 (SGK1). Biochem J 416:375–385

Goddard and Kneller (2008) SPARKY 3. University of California, San Francisco

Gottstein D, Reckel S, Dötsch V, Güntert P (2012) Requirements on paramagnetic relaxation enhancement data for membrane protein structure determination by NMR. Structure 20:1019–1027

Güntert P, Mumenthaler C, Wüthrich K (1997) Torsion angle dynamics for NMR structure calculation with the new program DYANA. J Mol Biol 273:283–298

Hayashi K, Kojima C (2008) pCold-GST vector: a novel cold-shock vector containing GST tag for soluble protein production. Protein Expr Purif 62:120–127

Herrmann T, Güntert P, Wüthrich K (2002) Protein NMR structure determination with automated NOE assignment using the new software CANDID and the torsion angle dynamics algorithm DYANA. J Mol Biol 319:209–227

Holm L (2010) Dali server: conservation mapping in 3D. Nucleic Acids Res 38(Web Server issue):W545–W549

Holm L, Kääriäinen S, Rosenström P, Schenkel A (2008) Searching protein structure databases with DaliLite v. 3. Bioinformatics 24(23):2780–2781

Hresko RC, Mueckler M (2005) mTOR.RICTOR is the Ser473 kinase for Akt/protein kinase B in 3T3-L1 adipocytes. J Biol Chem 280:40406–40416

Hu JS, Bax A (1997) Chi 1 angle information from a simple two-dimensional NMR experiment that identifies trans $^{3}J_{NC}$ gamma couplings in isotopically enriched proteins. J Biomol NMR 9:323–328

Huang YJ, Swapna GV, Rajan PK, Ke H, Xia B, Shukla K, Inouye M, Montelione GT (2003) Solution NMR structure of ribosome-binding factor A (RbfA), a cold-shock adaptation protein from *Escherichia coli*. J Mol Biol 327:521–536

Ikeda K, Morigasaki S, Tatebe H, Tamanoi F, Shiozaki K (2008) Fission yeast TOR complex 2 activates the AGC-family Gad8 kinase essential for stress resistance and cell cycle control. Cell Cycle 7:358–364

Jacinto E, Facchinetti V, Liu D, Soto N, Wei S, Jung SY, Huang Q, Qin J, Su B (2006) SIN1/MIP1 maintains rictor-mTOR complex integrity and regulates Akt phosphorylation and substrate specificity. Cell 127:125–137

Jee J, Güntert P (2003) Influence of the completeness of chemical shift assignments on NMR structures obtained with automated NOE assignment. J Struct Funct Genom 4:179–189

Johnson B, Blevins R (1994) NMRView—a computer-program for the visualization and analysis of NMR data. J Biomol NMR 4:603–614

Kataoka S, Furuita K, Hattori Y, Kobayashi N, Ikegami T, Shiozaki K, Fujiwara T , Kojima C (2014) ^{1}H, ^{15}N and ^{13}C resonance assignments of the conserved region in the middle domain of *S. pombe* Sin1 protein. Biomol NMR Assign. doi:10.1007/s12104-014-9550-6

Kay LE, Torchia DA, Bax A (1989) Backbone dynamics of proteins as studied by 15 N inverse detected heteronuclear NMR spectroscopy: application to staphylococcal nuclease. Biochemistry 28:8972–8979

Kobayashi N, Iwahara J, Koshiba S, Tomizawa T, Tochio N, Güntert P, Kigawa T, Yokoyama S (2007) KUJIRA, a package of integrated modules for systematic and interactive analysis of NMR data directed to high-throughput NMR structure studies. J Biomol NMR 39:31–52

Liang B, Bushweller JH, Tamm LK (2006) Site-directed parallel spin-labeling and paramagnetic relaxation enhancement in structure

determination of membrane proteins by solution NMR spectroscopy. J Am Chem Soc 128:4389–4397

Madl T, Felli IC, Bertini I, Sattler M (2010) Structural analysis of protein interfaces from ^{13}C direct-detected paramagnetic relaxation enhancements. J Am Chem Soc 132:7285–7287

Madl T, Güttler T, Görlich D, Sattler M (2011) Structural analysis of large protein complexes using solvent paramagnetic relaxation enhancements. Angew Chem Int Ed Engl 50:3993–3997

Matsuo T, Kubo Y, Watanabe Y, Yamamoto M (2003) *Schizosaccharomyces pombe* AGC family kinase Gad8p forms a conserved signaling module with TOR and PDK1-like kinases. EMBO J 22:3073–3083

Muhandiram D, Farrow N, Xu G, Smallcombe S, Kay L (1993) A gradient C-13 NOESY-HSQC experiment for recording noesy spectra of C-13-labeled proteins dissolved in H_2O. J Magn Reson Ser B 102:317–321

Murzin AG, Brenner SE, Hubbard T, Chothia C (1995) SCOP: a structural classification of proteins database for the investigation of sequences and structures. J Mol Biol 247(4):536–540

Nilges M (1997) Ambiguous distance data in the calculation of NMR structures. Fold Des 2:S53–S57

Ottiger M, Delaglio F, Bax A (1998) Measurement of J and dipolar couplings from simplified two-dimensional NMR spectra. J Magn Reson 131:373–378

Reckel S, Gottstein D, Stehle J, Loehr F, Verhoefen M-K, Takeda M, Silvers R, Kainosho M, Glaubitz C, Wachtveitl J, Bernhard F, Schwalbe H, Guentert P, Doetsch V (2011) Solution NMR structure of proteorhodopsin. Angew Chem Int Ed 50:11942–11946

Roosild TP, Greenwald J, Vega M, Castronovo S, Riek R, Choe S (2005) NMR structure of Mistic, a membrane-integrating protein for membrane protein expression. Science 307:1317–1321

Sarbassov DD, Guertin DA, Ali SM, Sabatini DM (2005) Phosphorylation and regulation of Akt/PKB by the rictor-mTOR complex. Science 307:1098–1101

Schwieters CD, Kuszewski JJ, Tjandra N, Clore GM (2003) The Xplor-NIH NMR molecular structure determination package. J Magn Reson 160(1):65–73

Schwieters CD, Kuszewski JJ, Clore GM (2006) Using Xplor-NIH for NMR molecular structure determination. Progr NMR Spectrosc 48:47–62

Shen Y, Delaglio F, Cornilescu G, Bax A (2009) TALOS+ : a hybrid method for predicting protein backbone torsion angles from NMR chemical shifts. J Biomol NMR 44:213–223

Simon B, Madl T, Mackereth CD, Nilges M, Sattler M (2010) An efficient protocol for NMR-spectroscopy-based structure determination of protein complexes in solution. Angew Chem Int Ed Engl 49:1967–1970

Van Horn WD, Kim H-J, Ellis CD, Hadziselimovic A, Sulistijo ES, Karra MD, Tian C, Soennichsen FD, Sanders CR (2009) Solution nuclear magnetic resonance structure of membrane-integral diacylglycerol kinase. Science 324:1726–1729

Volkov AN, Worrall JAR, Holtzmann E, Ubbink M (2006) Solution structure and dynamics of the complex between cytochrome c and cytochrome c peroxidase determined by paramagnetic NMR. Proc Natl Acad Sci 103:18945–18950

Wullschleger S, Loewith R, Hall MN (2006) TOR signaling in growth and metabolism. Cell 124:471–484

Yang Q, Inoki K, Ikenoue T, Guan KL (2006) Identification of Sin1 as an essential TORC2 component required for complex formation and kinase activity. Genes Dev 20:2820–2832

Yang Y, Ramelot TA, McCarrick RM, Ni S, Feldmann EA, Cort JR, Wang H, Ciccosanti C, Jiang M, Janjua H, Acton TB, Xiao R, Everett JK, Montelione GT, Kennedy MA (2010) Combining NMR and EPR methods for homodimer protein structure determination. J Am Chem Soc 132:11910–11913

Zhang O, Kay LE, Olivier JP, Forman-Kay JD (1994) Backbone ^{1}H and ^{15}N resonance assignments of the N-terminal SH3 domain of drk in folded and unfolded states using enhanced-sensitivity pulsed field gradient NMR techniques. J Biomol NMR 4:845–858

Zhou Y, Cierpicki T, Jimenez RH, Lukasik SM, Ellena JF, Cafiso DS, Kadokura H, Beckwith J, Bushweller JH (2008) NMR solution structure of the integral membrane enzyme DsbB: functional insights into DsbB-catalyzed disulfide bond formation. Mol Cell 31:896–908

Zweckstetter M, Bax A (2000) Prediction of sterically induced alignment in a dilute liquid crystalline phase: aid to protein structure determination by NMR. J Am Chem Soc 122:3791–3792